

Contents lists available at ScienceDirect

Photoacoustics

journal homepage: www.elsevier.com/locate/pacs



Research article

Side-viewing photoacoustic waveguide endoscopy

Christopher Miranda, Ethan Marschall, Blake Browning, Barbara S. Smith*

School of Biological and Health Systems Engineering, Arizona State University, Tempe, AZ 85281, USA



ARTICLE INFO

Keywords:
Photoacoustic endoscopy waveguide

ABSTRACT

Side-viewing hollow optical waveguides allow for minimally invasive endoscopy by concentrically guiding light and sound for photoacoustic generation and detection. Here, we characterize the side-viewing photoacoustic waveguide (PWG) endoscope by scanning 7.2 µm diameter carbon fiber threads within phantom tissues and animal tissues. Photoacoustic signals are carried along the 5.5 and 10.0 cm length of the PWG with minimal attenuation. Thus, this technology enables 360°, deep-tissue photoacoustic imaging. Photoacoustic signals were identified up to 8.0 mm from the PWG imaging window in an optically clear medium. The outer diameter of this device is measured as just over 1.0 mm, with the potential to be further miniaturized due to its unique design. The PWG is an ideal candidate for a myriad of pre-clinical and clinical applications where typical photoacoustic endoscopy systems are impractical, due to their size. Presented here, is the first side-viewing photoacoustic waveguide endoscope.

1. Introduction

Photoacoustic endoscopy (PAE) has emerged as a minimally invasive tool for imaging internal organs and tissues. Previous applications have successfully included imaging of the vasculature along the esophagus and intestines [1–5], plaque in large arteries [6–12], and the lining of the uterus [13]. For certain applications, however, further minimization is necessary [14,15].

PAE systems typically utilize imaging probes with diameters on the order of a few millimeters, capable of generating and detecting the photoacoustic effect in the radial direction. The photoacoustic effect being, in brief, the thermoelastic-induced creation of acoustic waves resulting from the absorption of photons by select targets. Additionally, a transducer, often located within the endoscope itself, is typically used to detect acoustic waves - with the size of the transducer affecting the signal-to-noise ratio [16]. Further minimization of PAE systems has often relied on downsizing the transducer, thus creating a difficult challenge for transducer manufacturers. This prevents scalability of traditional systems and limits their potential of being good candidates for pre-clinical and clinical applications. Alternative PAE architectures, however, may be able to circumvent these manufacturing issues by providing light transmission and sound detection on a significantly smaller size scale, thus mitigating the need for smaller transducers, and alleviating the challenges for manufacturers. The proposed alternate PAE method utilizes a hollow optical waveguide to allow for concentric guiding of both light and sound [17]. This enables photoacoustic detection with a transducer, distant from the imaging window, providing a further reduction in the scale of the endoscope. Capillaries (e.g. such as of borosilicate or quartz glass) can be used as hollow optical waveguides due to their material properties, where the glass wall allows for total internal reflection of an efficiently coupled light source. The use of capillary tubes as optical waveguides extends back several decades [18–21]. Similarly, transducers can be coupled to the water filled center of a hollow optical waveguide, enabling ultrasound travel of several centimeters along the length of a capillary with minimal attenuation. Recent attempts have been made to characterize the functionality of these hollow waveguides for use in PAE [22,23]. To date, however, all photoacoustic hollow waveguide endoscopy probes have been forward facing, thus limiting their usefulness in *in vivo* applications.

To combine the benefits of traditional side-viewing PAE with the miniaturization allowable by hollow optical waveguides, we investigate the use of side-viewing photoacoustic waveguide (PWG) endoscopes. The proposed side-viewing PWG architecture provides benefits over traditional PAE designs by enabling miniaturization without the need for highly specialized ultrasound transducers. Rather, the water filled hollow center of the PWG can be coupled to transducers of a range of size or frequency – allowing for versatility, unseen in prior PAE models. Thus, insertion of the hollow optical waveguide into tissue, allows for light delivery and sound detection at distances exceeding the depth of penetration for visible light and high-frequency ultrasound. This is accomplished through the use of an optical and acoustic combiner located

E-mail address: BarbaraSmith@asu.edu (B.S. Smith).

^{*} Corresponding author.

externally to the PWG and up to several centimeters from the imaging window. Thus, any noise that may be generated as a result of incident light on the transducer occurs well before acquisition of the signals of interest. PAE systems with improper optical and acoustic separation have led to ultrasound transducers being exposed to excitation light, resulting in bright rings in image reconstruction. This results in poor signal-to-noise ratio for photoacoustic signals acquired near the imaging window. Furthermore, rotation of the device allows for a 360° photoacoustic reconstruction with imaging depths approaching a centimeter. With a relatively inexpensive fabrication, the PWG is an ideal candidate for a myriad of pre-clinical and clinical applications where typical PAE systems are impractical, due to their size. As a result of the efficiency of PWG in transmitting both light and sound, further imaging modalities including fluorescence and pulse-echo ultrasound imaging may still be incorporated into the device.

2. Materials and methods

2.1. System architecture

The side-viewing PWG design was investigated for application as an *in vivo* imaging tool. The PWG architecture, depicted in Fig. 1(a), consists of a contained system for optical and acoustic coupling [Fig. 1(b)], O-ring system [Fig. 1(c)], and the PWG [Fig. 1(d)].

Photoacoustic imaging is initiated by a tunable LS-2134-LT40 Nd:YAG/Ti:Sapphire nanosecond pulsed laser (Symphotic TII Corporation) operated at a 532 nm wavelength. The laser provides an excitation light with a full width half maximum (FWHM) of 12–15 ns at a pulse repetition rate of 10 Hz. Light is focused into a multimode optical fiber using a 10× objective with a 0.25 NA (LMH-10X-532, Thorlabs). The optical fiber is coupled to the PWG using our custom design and built optical and acoustic coupling system [Fig. 1(b)], consisting of a custom 3D-printed water tank that holds a 1 mm thick glass slide positioned at a 45° angle relative to the center-line axis of the PWG. A small spot size of light is focused onto one portion of the capillary glass wall with a near-zero acceptance angle [17]. This is performed by using a second 10× objective with a 0.25 NA (LMH-10x-1064, Thorlabs), as depicted in Fig. 1(b).

Light continues along the glass wall of the PWG by total internal reflection through the O-ring system, as shown in Fig. 1(c). This system consists of two lubricated O-rings embedded within the holder and fixed in the bottom of the optical and acoustic coupling system. The rotational capability of the PWG is provided by a belt-system powered with a NEMA 17 Stepper Motor. The belt-system comprises a timing belt and timing pulleys, one attached to the external wall of the PWG and the other attached to the stepper motor. Thus, the O-ring system facilitates photoacoustic imaging in 360°, due to its ability to rotate the PWG about the center-line axis, while allowing for uninterrupted optical and acoustic coupling. Thus, the O-ring system allows 360° photoacoustic imaging, due to its ability to rotate the PWG about the center-line axis, while allowing for uninterrupted optical and acoustic coupling.

Light travels along the length of the PWG where it is ultimately redirected by a right angle prism, through optically clear medical tubing, and exits perpendicular to the center-line axis. The optical emission from the PWG presents itself as a Gaussian-like circular diverging beam. The PWG is composed of three primary components, including: (i) borosilicate glass capillary tubes (B100-75-10, Sutter Instrument), (ii) aluminum coated right angle prism (MPCH-1.0, Tower Optical), and (iii) medical tubing (103-0552, Vention Medical), as shown in Fig. 1(d). Light exiting the PWG can induce the photoacoustic effect. Resulting photoacoustic signals travel through the acoustically clear medical tubing and along the water filled core of the PWG. Sound travels back up the entire length of the PWG into the dual optical and acoustic coupling system. Sound is redirected toward the center of a submerged transducer positioned perpendicular to the center-line axis

of the PWG. The transducer has a center frequency of 10 MHz, a focal length of 1.27 cm, an element diameter of 6 mm, and a -6 dB fractional bandwidth of 99.9% (A312S-SU, Olympus). Photoacoustic signals detected by the transducer are sent to an ultrasound pulser/receiver (5077PR, Olympus Inc.), where amplification is performed through a 59 dB gain and filtered with a 1 MHz high pass filter to minimize the inherent low-frequency noise of the system. Data acquisition is performed with a multipurpose reconfigurable oscilloscope (NI PXIe-5170R, National Instruments Corporation) and transferred to a computer for image reconstruction. The multipurpose reconfigurable oscilloscope has built-in programmable function input/output (PFI) lines controlled by a built-in field programmable gate array (FPGA) allowing for custom triggering and synchronization of the system. A render of the side-viewing photoacoustic endoscopy system is shown in Fig. 2.

2.2. Phantom and animal models

To demonstrate the imaging capabilities of the PWG, the device is introduced into the hollow center of a cylindrical polyvinyl chloride plastisol (PVCP, M-F Manufacturing) phantom and scanned from within. Line targets, embedded vertically in the PVCP phantoms, are radially scanned using the methods depicted in Figs. 3(a) and (b). The PVCP phantoms are fabricated according to previous methods [13,24], with minor adjustments. In brief, 90 mL of PVCP is poured into a round bottom flask, submerged in an oil bath at 220 °C. The mixture is allowed to heat for approximately 9 min while stirring under vacuum. PVCP is transferred to a glass cylinder mold with a protruding center and parallel line targets. The PVCP remains in the mold until it reaches room temperature and solidifies. A cylindrical phantom with an outer diameter of 3.8 cm, inner diameter of 3 mm, and embedded line targets is shown in Fig. 3(c). Phantoms consisting of 7.2 μm diameter carbon fiber threads are positioned approximately 3 mm from the center of the mold, or 254 µm diameter carbon fiber rods are positioned approximately 6.5-8 mm from the mold center.

To demonstrate the clinical relevance of the PWG, further imaging studies were performed in animal tissue (chicken breast). The PWG was carefully inserted into the tissue sample along a pathway created by pre-insertion of an 18-gauge needle. Two $254\,\mu m$ diameter rods and a glass capillary tube filled with distilled water (negative control) were inserted into the tissue sample.

2.3. Illumination methods

Scans were first performed using external illumination on $7.2\,\mu m$ carbon fiber threads. To perform photoacoustic endoscopy using external illumination, an optical fiber was oriented perpendicularly to the imaging probe, aligned with the imaging window of the PWG, and positioned roughly 1 mm from the outer surface of the phantom tissue. This experimental setup is demonstrated in Fig. 3(a). Both the PWG and the optical fiber are fixed in position, while the phantom is rotated about its centerline axis using a custom built rotating stage.

Subsequent experiments were performed using internal illumination, where the phantom or animal model was fixed in position and the PWG was rotated about its centerline axis using a belt band system. This experimental setup is demonstrated in Fig. 3(b).

2.4. Reconstruction

Acquisitions are performed at 800 angular positions spanning a total of 360°. An analytical signal is created using each A-line acquisition, s (t), and its Hilbert transform, H[s(t)]. The magnitude of the analytical signal is calculated to create a complex envelope, $s_e(t)$, of each A-line acquisition such that $s_e(t) = \sqrt{s^2(t) + H^2[s(t)]}$. This envelope is then normalized based on the maximum value of the entire 2D scan and converted into a series of pixel values. Each processed A-line is

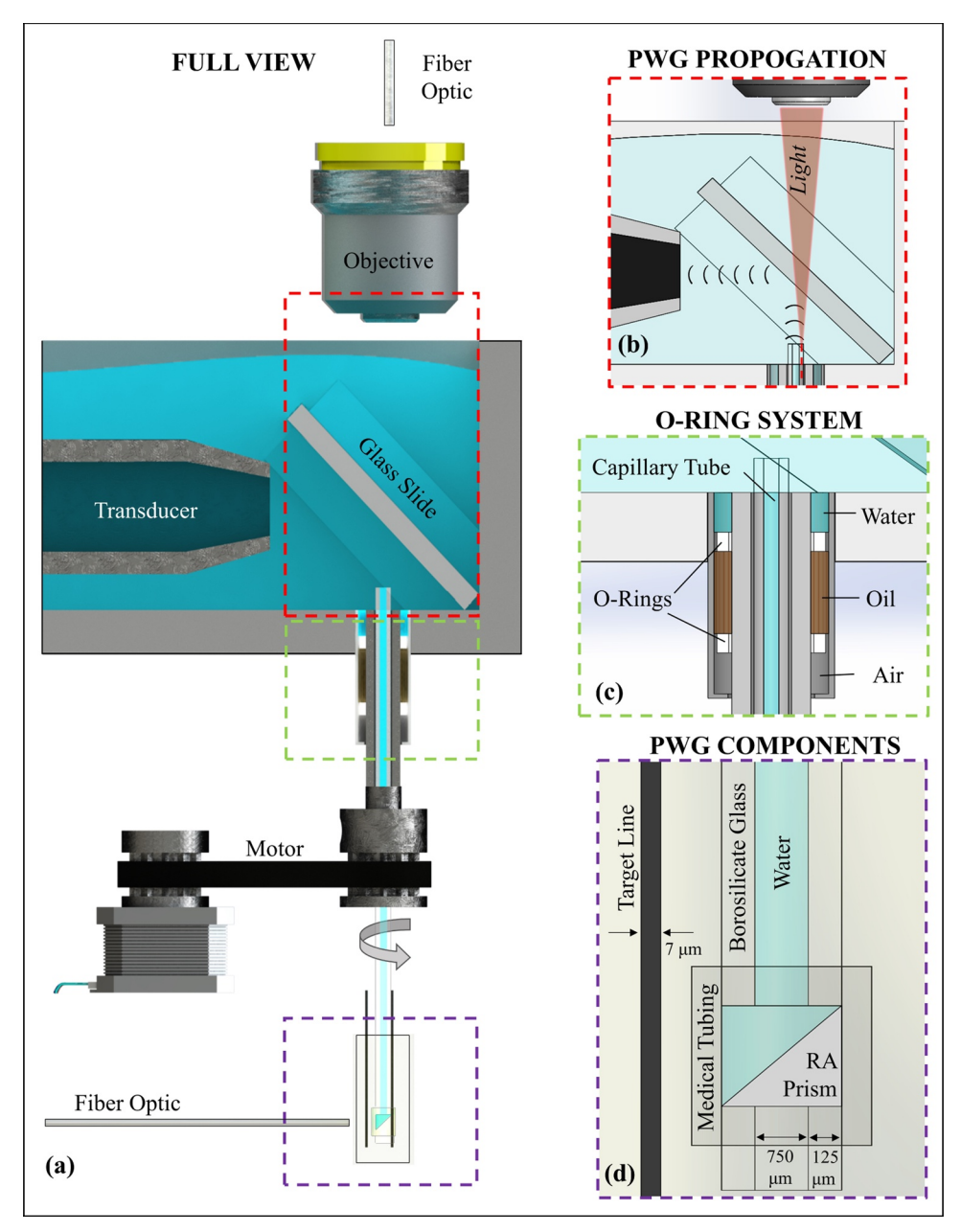


Fig. 1. (a) Full view of the PWG architecture. (b) Coupling system demonstration of the optical and acoustic coupling to the PWG. (c) O-ring system used to rotate PWG about its center-line axis. (d) Components of the PWG.

compressed to a total of 500 representative data points by averaging clusters of numbers together, thus resulting in representative A-lines with fewer data points. Using a look-up table format, each data point is assigned a group of pixels using a weighted average.

3. Results and discussion

3.1. Photoacoustic imaging in phantom tissue

Fig. 4(a) is a photoacoustic reconstruction of a 7.2 μ m diameter line targets embedded within a phantom tissue using external illumination. Measurements of the line target were performed in both the transverse and radial direction, as demonstrated by green dashed lines, as shown in Fig. 4(a). For transverse measurements, a maximum signal is identified at each angular step, normalized, and plotted, as shown in Fig. 4(b). The transverse FWHM is measured to be 1.0 mm using a Gaussian fit and a radial distance of 3 mm from the PWG. Radial

resolution measurements were performed on the A-line acquired at the angular step that provided the maximum signal. Using a Gaussian fit, the radial resolution measurement shows a FWHM of 386 μm using a speed of sound in the phantom of 1400 m/s.

Further transverse and radial measurements are performed on three, $254\,\mu m$ diameter carbon fiber rods using internal illumination by rotating PWG [Fig. 5(a)]. Comparison of these reconstructions demonstrates that the PWG is able to maintain efficient optical and acoustic coupling, while rotating about its axis. The maximum value is calculated and plotted at each angular step of the 360° scan, as shown in Fig. 5(b). In Fig. 5(b) the mean transverse FWHM is calculated to be 0.6 mm. Comparison of the FWHM using external and internal illumination suggests that resolution is determined by the spot size of the optical beam. In this configuration, the PWG is rotated within the fixed phantom in order to demonstrate clinical relevance of the endoscope. Measurements in the radial direction for each configuration are performed using the angular position corresponding to the maximum peak

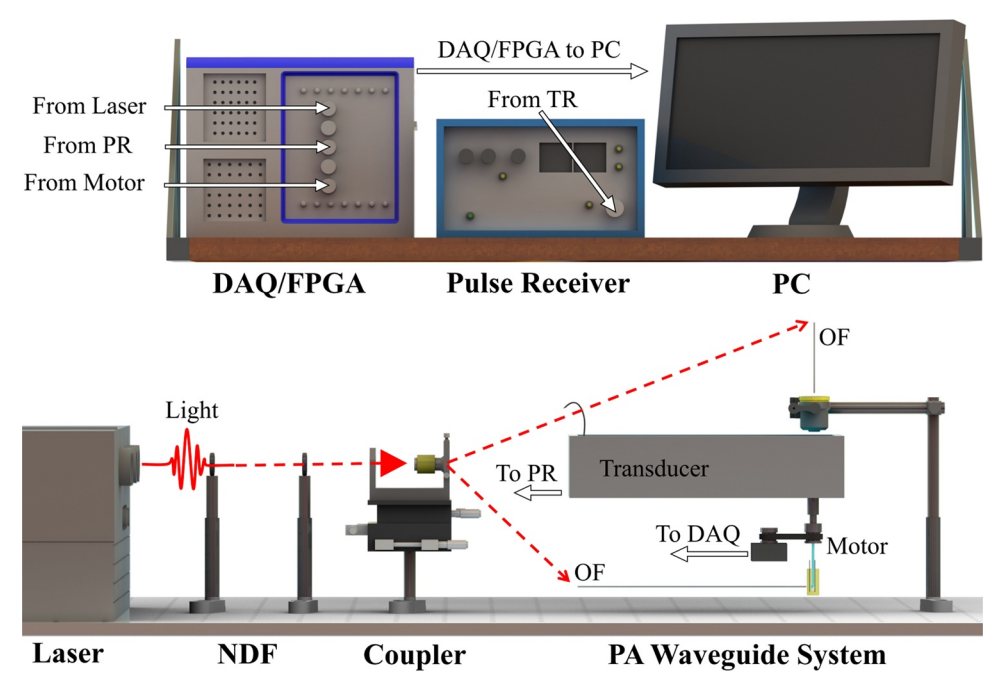


Fig. 2. Render showing the system architecture. NDF, neutral density filter; OF, optical fiber; PR, pulser receiver; DAQ/FPGA, data acquisition/field programmable gate array.

from each of the carbon fiber rods. The mean photoacoustic FWHM in the radial direction of Fig. 5(b) is calculated to be $567\,\mu m$. A representative signal is shown in Fig. 5(c), which corresponds to the largest peak in Fig. 5(b). Transverse resolution is dependent on light exiting the PWG. As the PWG system is optimized, the light may be more focused or collimated, improving transverse resolution [25]. Additionally, the waveguide diameter may be selected according to desired frequency of the transducer – a decrease in the frequency of the ultrasound would benefit from an increase in the diameter, and vice versa. This is not expected to have a direct effect on transverse resolution. If a higher frequency/bandwidth were used, the axial resolution would be increased.

Attenuation of sound through the side-viewing photoacoustic waveguide endoscope was measured to be approximately -18 and $-25\,\text{dB}$ for the 5.5 and $10.0\,\text{cm}$ length, respectively. The selection of a ubiquitous frequency is expected to allow for greater translation of the PWG paradigm. Thus, 10 MHz was selected as it is often utilized within ranges for PA imaging and is potentially well-understood. For both lengths, the optical coupling efficiency was $\sim\!37\%$. The energy output of the light that enters the PWG has been measured to be $49\,\mu\text{J}$. The energy output of the light that exits the PWG at the phantom interface

has been measured to be $18 \,\mu J$. The PWG has been demonstrated with a laser energy fluence of $\sim 1.8 \, mJ/cm^2$, which remains below the laser safety standard of $20 \, mJ/cm^2$ [26].

3.2. Photoacoustic imaging in animal tissue

Results indicated that 2 mm was the approximate maximum imaging distance in the tissue sample. The targets were scanned in the method depicted in Fig. 6(a). Rotation of the PWG from the proximal end resulted in equal rotation on the distal, end while in contact with the tissue sample. This suggests that the 6 μ m thick medical tubing is able to withstand twisting of the PWG during imaging. The photoacoustic reconstruction of the carbon fiber rods in animal tissue are shown in Fig. 6(b). Excluding the first microsecond of each acquisition, the maximum signal per acquisition was plotted in Fig. 6(c). The mean transverse FWHM is calculated to be 514 μ m. Measurements in the radial direction for each configuration are performed using the angular position corresponding to the maximum peak from each of the carbon fiber rods. The mean photoacoustic FWHM in the radial direction of Fig. 6(a) was calculated to be 436 μ m, assuming a speed of sound in the tissue of 1540 m/s. A representative signal is shown in Fig. 6(d), which

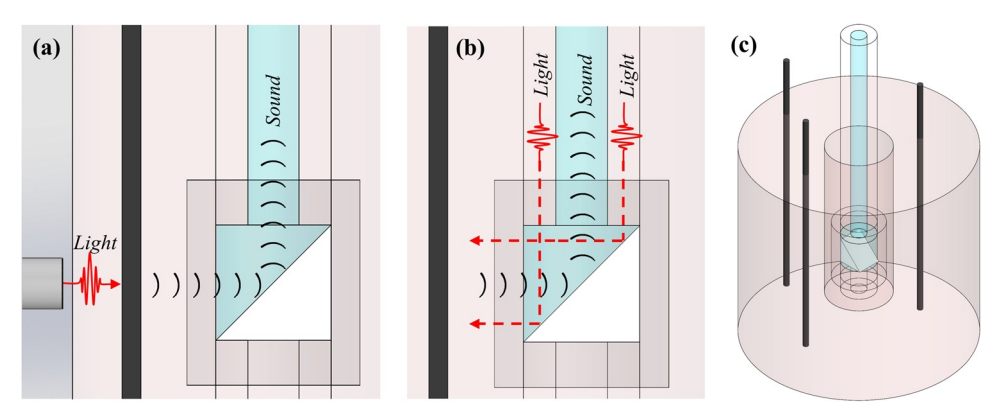


Fig. 3. (a) Schematic demonstrating experimental setup for external illumination to generate the photoacoustic effect from the line target. (b) Schematic demonstrating experimental setup for internal illumination. (c) CAD model of phantom with 254 μm carbon fiber rods.

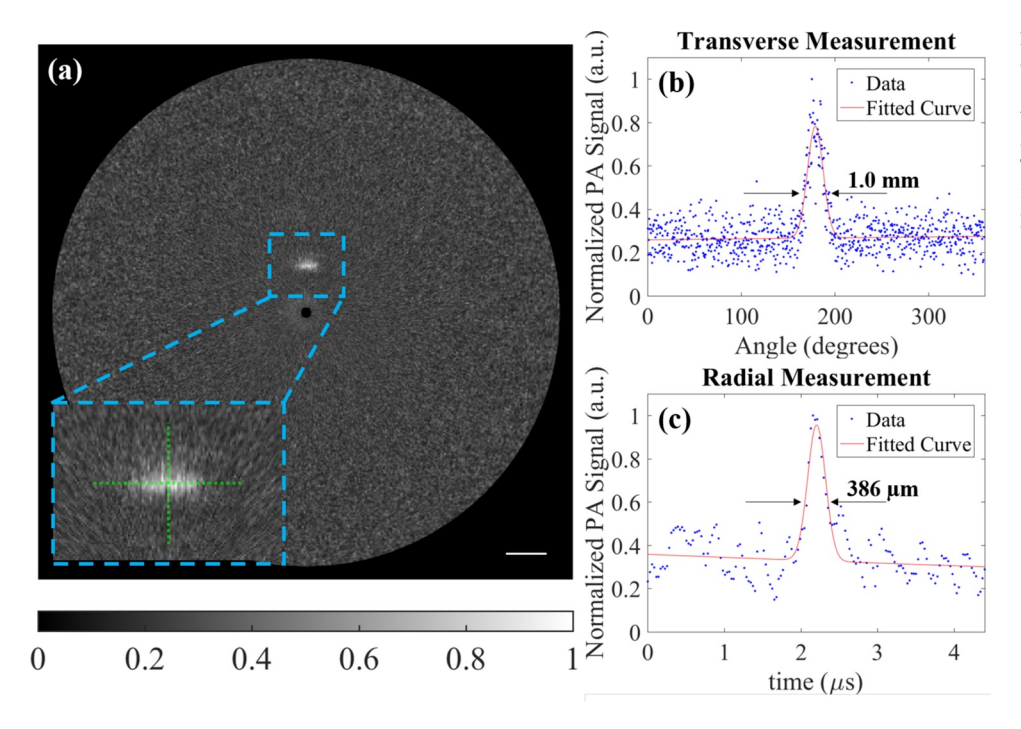


Fig. 4. (a) Photoacoustic image reconstruction of $7.2\,\mu m$ thread at a distance of approximately 3 mm from imaging probe. Horizontal and vertical green dashed lines represent transverse and radial measurements, respectively. (b) Transverse resolution measurement of thread in (a). (c) Radial resolution measurement of peak signal in (b). Scale bar represents 3 mm.

corresponds to the largest peak in Fig. 6(c). This resolution may be suitable for larger vasculature [27]. However, further improvements to the resolution are necessary in order to properly image microvasculature [28,29].

4. Conclusions

Our results demonstrate a side-viewing PWG design which enables minimally invasive photoacoustic imaging without the need for highly specialized transducers or acoustic detectors, common to most miniaturized PAE systems. The lack of direct transducer contact reduced the size of the PWG due to enabling for both light and sound translation across the length of the probe. This design allows for all components of the probe to fit within a diameter of 1 mm which is comparable to the range of recently published endoscopic photoacoustic imaging systems [5,11,12]. One limitation to the PWG design is that decreasing the radius, r, decreases the cross sectional area over which sound can propagate as a function of $1/r^2$ which may ultimately result in a large decrease in sensitivity. Moreover, further work is needed to determine the theoretical limit of PWG size. It is expected that a decrease in diameter will reduce the allowable range of transducer frequencies. A possible application of the PWG is in deep brain stimulation (DBS) surgeries, performed by inserting electrodes into select regions in the brain of a patient. Sufficiently small PWG diameters may allow for the possibility of combining the imaging probe with DBS electrodes for real-time intraoperative imaging. Additionally, the capacity for realtime side viewing endoscopy during DBS electrode placement would enable the identification of landmarks to determine the spatial location of the electrode. Due to the fact that our design does not require the transducer to be located inside the PWG itself, further miniaturization of the device may only be limited by the amount of sound and light that can travel along the axis of the imaging probe. Further optimization of the current system is possible. For example, the addition of an external aluminum coating [30] or wave-front shaping [31] may provide improved light coupling efficiency with wavelengths in the vis-NIR. The substitution to quartz glass (e.g. capillary tube and glass slide) may also improve transmission efficiency. The expected change in transmission between visible to NIR is minimal. In most photoacoustic and ultrasound endoscopy imaging probes the imaging depth is ultimately constrained to a few millimeters [2,32,33]. As the PWG energy fluence of 1.8 mJ/cm² is below the laser safety standard of 20 mJ/cm², more energy into the system is allowable. Future studies will investigate the effects of PWG energy fluence on SNR. Further depth may be achieved through selecting a longer wavelength. Further optimization to reduce attenuation of sound may be achievable through proper selection of transducer frequency. This work highlights the design, development, and the current capabilities of the first ever side-viewing PWG device. Further work will aim to improve transverse resolution and incorporate

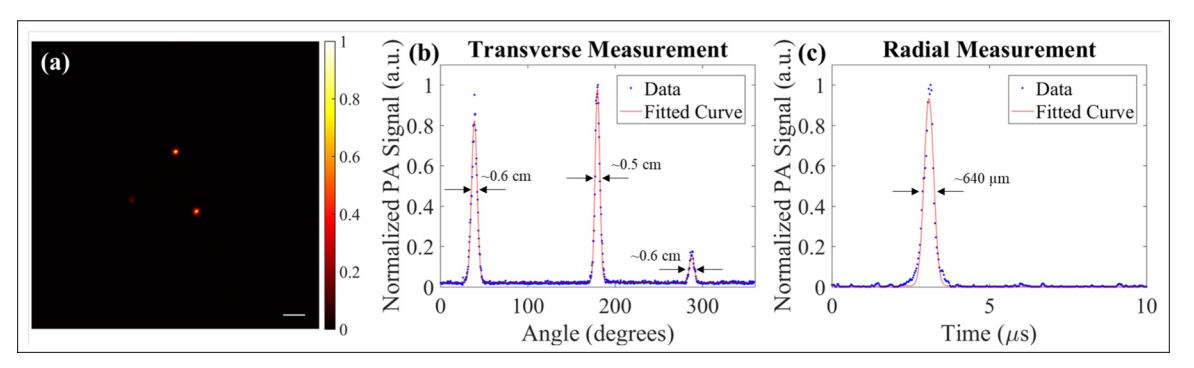


Fig. 5. Photoacoustic reconstructions using internal illumination with rotating PWG. Scale bar represent 3 mm. Color bar represent normalized photoacoustic amplitude. (b) Maximum amplitude plot at each angular position. (c) Acquisitions corresponding to max signals in (b).

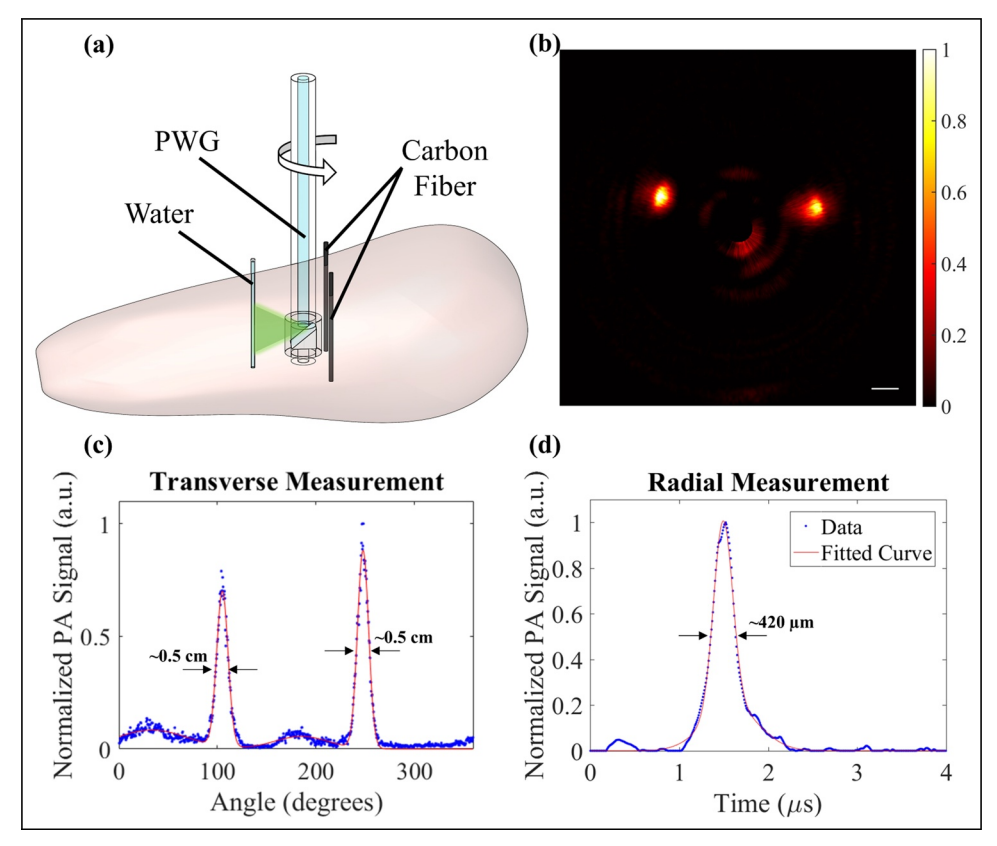


Fig. 6. (a) Schematic representation of experimental setup performed within chicken breast. (b) Photoacoustic reconstruction clearly showing the two carbon fiber targets. Scale bar represents 1 mm. (c) Maximum amplitude plot of each angular position in (b). (d) Radial measurement of largest signal in (c).

fluorescence, photoacoustic contrast agents, and pulse-echo ultrasound imaging for use in *in vivo* biomedical applications.

Conflict of interest

None declared.

Acknowledgments

We thank Michael Sobrado for his technical assistance.

References

- [1] J.M. Yang, C. Favazza, J. Yao, R. Chen, Q. Zhou, K.K. Shung, L.V. Wang, Three-dimensional photoacoustic endoscopic imaging of the rabbit esophagus, PLOS ONE 10 (4) (2015) e0120269.
- [2] J.-M. Yang, C. Favazza, R. Chen, J. Yao, X. Cai, K. Maslov, Q. Zhou, K.K. Shung, L.V. Wang, Simultaneous functional photoacoustic and ultrasonic endoscopy of internal organs in vivo, Nat. Med. 18 (8) (2012) 1297–1302.
- [3] J.-M. Yang, C. Favazza, R. Chen, K. Maslov, X. Cai, Q. Zhou, K.K. Shung, L.V. Wang, Volumetric photoacoustic endoscopy of upper gastrointestinal tract: ultrasonic transducer technology development, Proc. SPIE, Vol. 7899 (2011) 78990D1–78990D6.
- [4] J.-M. Yang, K. Maslov, H.-C. Yang, Q. Zhou, K.K. Shung, L.V. Wang, Photoacoustic endoscopy, Opt. Lett. 34 (10) (2009) 1591–1593.
- [5] Y. Li, G. Lu, J.J. Chen, J.C. Jing, T. Huo, R. Chen, L. Jiang, Q. Zhou, Z. Chen, PMN-PT/epoxy 1-3 composite based ultrasonic transducer for dual-modality photo-acoustic and ultrasound endoscopy, Photoacoustics (2019) 100138.
- [6] A.B. Karpiouk, B. Wang, J. Amirian, R.W. Smalling, S.Y. Emelianov, Feasibility of in vivo intravascular photoacoustic imaging using integrated ultrasound and photoacoustic imaging catheter, J. Biomed. Opt. 17 (9) (2012) 0960081–0960086.
- [7] B. Wang, J.L. Su, A.B. Karpiouk, K.V. Sokolov, R.W. Smalling, S.Y. Emelianov, Intravascular photoacoustic imaging, IEEE J. Sel. Top. Quant. Electron. 16 (3) (2010) 588–599.
- [8] B. Wang, A. Karpiouk, D. Yeager, J. Amirian, S. Litovsky, R. Smalling, S. Emelianov, Intravascular photoacoustic imaging of lipid in atherosclerotic plaques in the presence of luminal blood, Opt. Lett. 37 (7) (2012) 1244–1246.
- [9] P. Wang, T. Ma, M.N. Slipchenko, S. Liang, J. Hui, K.K. Shung, S. Roy, M. Sturek, Q. Zhou, Z. Chen, J.-X. Cheng, High-speed intravascular photoacoustic imaging of

- lipid-laden atherosclerotic plaque enabled by a 2-kHz barium nitrite Raman laser, Sci. Rep. 4 (2014) 6889.
- [10] E.Z. Zhang, P.C. Beard, A miniature all-optical photoacoustic imaging probe, Proc. SPIE, Vol. 7899 (2011) 78991F.
- [11] S. Iskander-Rizk, M. Wu, G. Springeling, F. Mastik, R.H. Beurskens, A.F. van der Steen, G. van Soest, Catheter design optimization for practical intravascular photoacoustic imaging (IVPA) of vulnerable plaques, Diagnostic and Therapeutic Applications of Light in Cardiology 2018, Vol. 10471 (2018) 1047111.
- [12] C. Shu, Z. Xie, D. Yang, Z. Chen, L. Song, X. Gong, High-speed intravascular photoacoustic imaging with blood flushing, Optics in Health Care and Biomedical Optics IX, Vol. 11190 (2019) 111901V.
- [13] C. Miranda, J. Barkley, B.S. Smith, Intrauterine photoacoustic and ultrasound imaging probe, J. Biomed. Opt. 23 (4) (2018) 46008.
- [14] P. Kim, E. Chung, H. Yamashita, K.E. Hung, A. Mizoguchi, R. Kucherlapati, D. Fukumura, R.K. Jain, S.H. Yun, In vivo wide-area cellular imaging by side-view endomicroscopy, Nat. Methods 7 (4) (2010) 303.
- [15] H. Ramakonar, B.C. Quirk, R.W. Kirk, J. Li, A. Jacques, C.R. Lind, R.A. McLaughlin, Intraoperative detection of blood vessels with an imaging needle during neurosurgery in humans, Sci. Adv. 4 (12) (2018) eaav4992.
- [16] Q. Zhou, K.H. Lam, H. Zheng, W. Qiu, K.K. Shung, Piezoelectric single crystal ultrasonic transducers for biomedical applications, Prog. Mater. Sci. 66 (2014) 87–111.
- [17] C. Miranda, S. Sampath Kumar, J. Muthuswamy, B.S. Smith, Photoacoustic micropipette, Appl. Phys. Lett. 113 (26) (2018) 264103.
- [18] Y. Matsuura, T. Abel, J. Hirsch, J. Harrington, Small-bore hollow waveguide for delivery of near singlemode IR laser radiation, Electron. Lett. 30 (20) (1994) 1688–1690.
- [19] Y. Matsuura, T. Abel, J.A. Harrington, Optical properties of small-bore hollow glass waveguides, Appl. Opt. 34 (30) (1995) 6842–6847.
- [20] R.L. Kozodoy, A.T. Pagkalinawan, J.A. Harrington, Small-bore hollow waveguides for delivery of 3-µm laser radiation, Appl. Opt. 35 (7) (1996) 1077–1082.
- [21] Y. Abe, Y.-W. Shi, Y. Matsuura, M. Miyagi, Flexible small-bore hollow fibers with an inner polymer coating, Opt. Lett. 25 (3) (2000) 150–152.
- [22] O. Simandoux, N. Stasio, J. Gateau, J.-P. Huignard, C. Moser, D. Psaltis, E. Bossy, Optical-resolution photoacoustic imaging through thick tissue with a thin capillary as a dual optical-in acoustic-out waveguide, Appl. Phys. Lett. 106 (9) (2015) 94102.
- [23] N. Stasio, A. Shibukawa, I.N. Papadopoulos, S. Farahi, O. Simandoux, J.-P. Huignard, E. Bossy, C. Moser, D. Psaltis, Towards new applications using capillary waveguides, Biomed. Opt. Express 6 (12) (2015) 4619–4631.
- [24] S.E. Bohndiek, S. Bodapati, D. Van De Sompel, S.-R. Kothapalli, S.S. Gambhir, Development and application of stable phantoms for the evaluation of photoacoustic imaging instruments, PLOS ONE 8 (9) (2013) e75533.
- [25] P. Beard, Biomedical photoacoustic imaging, Interface Focus (2011) rsfs20110028.

[26] AMERICAN NATIONAL STANDArd Institute, American National Standard for Safe Use of Lasers, Laser Institute of America, 2007.

- [27] J.M. Serrador, P.A. Picot, B.K. Rutt, J.K. Shoemaker, R.L. Bondar, MRI measures of middle cerebral artery diameter in conscious humans during simulated orthostasis, Stroke 31 (7) (2000) 1672–1678.
- [28] Y. Sekiguchi, H. Takuwa, H. Kawaguchi, T. Kikuchi, E. Okada, I. Kanno, H. Ito, Y. Tomita, Y. Itoh, N. Suzuki, et al., Pial arteries respond earlier than penetrating arterioles to neural activation in the somatosensory cortex in awake mice exposed to chronic hypoxia: an additional mechanism to proximal integration signaling? J. Cereb. Blood Flow Metab. 34 (11) (2014) 1761–1770.
- [29] C. Yeh, B.T. Soetikno, S. Hu, K.I. Maslov, L.V. Wang, Microvascular quantification based on contour-scanning photoacoustic microscopy, J. Biomed. Opt. 19 (9) (2014) 96011.
- [30] Y.-W. Shi, K. Ito, L. Ma, T. Yoshida, Y. Matsuura, M. Miyagi, Fabrication of a polymer-coated silver hollow optical fiber with high performance, Appl. Opt. 45 (26) (2006) 6736–6740.
- [31] R. Horstmeyer, H. Ruan, C. Yang, Guidestar-assisted wavefront-shaping methods for focusing light into biological tissue, Nat. Photon. 9 (9) (2015) 563.
- [32] S. Sethuraman, S.R. Aglyamov, J.H. Amirian, R.W. Smalling, S.Y. Emelianov, Intravascular photoacoustic imaging using an IVUS imaging catheter, IEEE Trans. Ultrason. Ferroelectr. Freq. Control 54 (5) (2007).

[33] K. Jansen, M. Wu, A.F. van der Steen, G. van Soest, Lipid detection in atherosclerotic human coronaries by spectroscopic intravascular photoacoustic imaging, Opt. Express 21 (18) (2013) 21472–21484.



Barbara S. Smith joined Arizona State University's School of Biological and Health Systems Engineering as an Assistant Professor in January 2015. The Smith Laboratory focuses on engineering solutions to better diagnose problems associated with women's health and mental illness. Ongoing research in her lab aims to develop novel imaging technologies and utilize multiomic analysis to forge entirely new paths towards early stage detection and diagnostic monitoring. Her overarching goal is to translate research and clinical technologies created in the lab for improved patient outcomes. Recent work in the Smith Lab, on photoacoustic waveguides, has led to the publication of a featured article in Applied Physics Letters. Smith has received

the NSF CAREER Award, Centennial Professorship Award, New Innovator Award from the Arizona Biomedical Research Consortion, and the NSF I-Corps Award for translational research, among others.